FULL PAPER

Dalton
www.rsc.org/dalton

Metal-ligated induced structural interconversion between $Pd_{23}(CO)_{20}(PEt_3)_{10}$ and $Pd_{23}(CO)_{20}(PEt_3)_8$ possessing highly dissimilar Pd_{23} core-geometries

Eugeny G. Mednikov, Sergei A. Ivanov, Jatuporn Wittayakun and Lawrence F. Dahl
Department of Chemistry, University of Wisconsin-Madison, Madison, WI 53706, USA

Received 17th February 2003, Accepted 6th March 2003
First published as an Advance Article on the web 19th March 2003

A $^{31}P\{^1H\}$ NMR study has conclusively established that $Pd_{23}(CO)_{20}(PEt_3)_{10}$ (**1**) and $Pd_{23}(CO)_{20}(PEt_3)_8$ (**2**), which differ by only two phosphine ligands, can be chemically induced in solution to interconvert reversibly into each other despite their having highly different metal-core geometries: *viz*., a centered hexacapped cuboctahedral Pd_{19} kernel (pseudo-O_h) with four wingtip Pd atoms in **1** versus a highly deformed centered hexacapped cubic Pd_{15} kernel (pseudo-D_{2d}) with eight capping Pd atoms in **2**. A structural diagram is given that shows a plausible *hypothetical* pathway for the geometrical transformation of **1** into **2** (or **2** into **1**) upon removal (or addition) of the two phosphine ligands. Although there is no experimental evidence indicating whether these chemically induced conversions are *inter*molecular or *intra*molecular, the proposed *intra*molecular interconversion emphasizes the major structural differences that exist between **1** and **2**. Complete interconversions of **2** into **1** (and **1** into **2**) were accomplished by $^{31}P\{^1H\}$ NMR-monitored reactions carried out within NMR tubes. Addition of "free" PEt_3 to **2** rapidly converts it into **1**; if an excess of PEt_3 is added, product **1** slowly transforms into the icosahedral-based $Pd_{16}(CO)_{13}(PEt_3)_9$ (**3**). Addition of O_2 (air) to **1** converts it into **2** and the phosphine oxide byproduct (Et_3PO), but the rate of this reverse chemical reaction is not nearly as fast; an excess of O_2 (air) also slowly converts **3**, if present in the reaction mixture, into **2**; the relatively slow rates of reactions involving **3** are attributed to the icosahedral-based Pd_{16} nuclearity in **3** being unlike the identical Pd_{23} nuclearities in **1** and **2**. In contrast to the chemically induced interconversion reactions between **1** and **2**, both the reaction of **1** with excess PEt_3 to form **3** and the reaction of **3** to form **2** are not quantitative. These facile interconversions provide a striking illustration concerning the abnormal capacity of ligated palladium clusters to undergo major changes in metal-core geometries upon addition/removal of ligands. This exceptional behavior may be readily attributed to the markedly weaker M–M and M–CO bonding interactions in palladium carbonyl clusters compared to those in nickel and platinum carbonyl clusters.

Introduction

Palladium is an exceptionally versatile transition metal in forming an unusually large number of homopalladium phosphine carbonyl clusters with a remarkable diversity of different metal-core geometries. Crystallographically determined high-nuclearity homopalladium clusters (*i.e*., those arbitrarily designated by us to have at least 10 metal-core atoms with direct metal–metal bonding) possess 16 distinctly different palladium core-geometries with n = 10,[1] 12,[2,3] 16,[4,5] 23 (**1**),[6–9] 23 (**2**),[10] 29,[3] 30,[11] 34,[9a] 35,[5] 38,[9] 39,[5] 52,[12] 54,[11] 59,[5,13] 66,[12] and 145.[14] All but two of these highly condensed metal-core frameworks have close-packed geometries containing metal fragments whose structural units may be described in terms of either ccp and mixed ccp/hcp stacking layers (including particular sequences corresponding to capping monoctahedra, cuboctahedra, and truncated ν_3-octahedra) or icosahedra. [One exception is the Pd_{38} cluster[9,15] that has a highly irregular metal-core geometry reported to be "complex, and cannot be described in terms of close-packing without invoking considerable distortion";[15d] the other exception is the highly deformed (body-centered) cubic-based Pd_{23} (**2**) cluster (*vide infra*)]. These structural units may also encompass "twinned" metal-core geometries possessing interpenetrating cuboctahedra,[11] interpenetrating centered icosahedra,[5] and one face-fused icosahedral/octahedral architecture (*viz*., Pd_{59}) composed of two centered icosahedra that *trans*-cap one bioctahedron.[5,13]

Conspicuous among the above listed homopalladium clusters are two Pd_{23} clusters, $Pd_{23}(CO)_{20}(PEt_3)_{10}$ (**1**)[6–9] and $Pd_{23}(CO)_{20}(PEt_3)_8$ (**2**),[10a] having metal cores with the same nuclearity but with greatly different metal frameworks. Crystal structures of both $Pd_{23}(CO)_{20}(PEt_3)_{10}$ (**1**)[6–8] and $Pd_{23}(CO)_{20}(PEt_3)_8$ (**2**)[10a] were established from X-ray diffraction studies; the triisopropylphosphine analogue of **2** was recently prepared and found from an X-ray crystallographic analysis[10b] to have a metal-core architecture closely resembling that of the triethylphosphine **2**. In sharp contrast to the well-known cuboctahedral-based metal-core geometry of $Pd_{23}(CO)_{20}(PEt_3)_{10}$ (**1**),[6,11,15] the relatively unknown metal framework of $Pd_{23}(CO)_{20}(PEt_3)_8$ (**2**) was previously described[10a,15d] only in general terms as "a fragment of body-centered cubic packing which has 14 Pd atoms in the nearest coordination environment around a central Pd atom". These metal-core descriptions of the two Pd_{23} clusters do not elucidate any seemingly possible architectural connection between their two metal-core geometries.

Previous documented examples of chemically induced transformations between different palladium carbonyl phosphine clusters can be divided into three classes:

(1) Transformations between clusters with *different* metal-core nuclearities due to addition/removal of ligand(s), as shown[1a] for

$$2Pd_{10}(CO)_{12}(PAlk_3)_6 + CO + 8PAlk_3 \longrightarrow 5Pd_4(CO)_5(PAlk_3)_4$$

$$5Pd_4(CO)_5(PAlk_3)_4 + 8H^+ \longrightarrow 2Pd_{10}(CO)_{12}(PAlk_3)_6 + CO + 8HPAlk_3^+$$

(where Alk denotes Et or Bu^n)

Similar reactions were carried out for interconversion between $Pd_{10}(CO)_{12}(PPh_3)_6$ and $Pd_4(CO)_5(PPh_3)_4$.[1c] The rapid chemical transformation in solution of $Pd_{10}(CO)_{12}(PBu_3)_6$ into $Pd_4(CO)_5(PBu_3)_4$ under a CO atmosphere was also studied preparatively;[1a] no intermediate species (*e.g*., a Pd_7 cluster) was isolated during the interconversion of these two molecular compounds in spite of their presumably complex intermolecular mechanism. $^{31}P\{^1H\}$ NMR was used to characterize each compound.[1e]

DOI: 10.1039/b301872p

(2) Transformations under a CO atmosphere between clusters with the *same* metal-core nuclearities (due to ligand substitution) where the core-geometry is *retained*, as shown [1a] for

$$Pd_{10}(CO)_{12}(PBu_3)_6 + 2CO + 2H^+ \longrightarrow Pd_{10}(CO)_{14}(PBu_3)_4 + 2HPBu_3^+$$

$$Pd_{10}(CO)_{14}(PBu_3)_4 + 2PBu_3 \longrightarrow Pd_{10}(CO)_{12}(PBu_3)_6 + 2CO$$

(3) Transformations between clusters with the *same* metal-core nuclearities [due to addition/removal of ligand(s)] where the core-geometry *changes*, as shown [1a,16] for

$$Pd_4(CO)_5(PBu_3)_4 + CO \rightleftharpoons Pd_4(CO)_6(PBu_3)_4$$

butterfly tetrahedron

Noteworthy for the third-class example is the comment [15d] that "this change in metal geometry on the reversible addition of a ligand is unusual".

Compelling evidence for the conversion of $Pd_{23}(CO)_{20}(PR_3)_{10}$ into $Pd_{23}(CO)_{20}(PR_3)_8$ was initially obtained from a $^{31}P\{^1H\}$ NMR spectrum of tri(n-butyl)phosphine $Pd_{23}(CO)_{20}(PBu^n_3)_{10}$ [6c,7] dissolved in C_6D_6 and then exposed to O_2 (air). The resulting spectrum [17] displayed singlets characteristic of $Pd_{23}(CO)_{20}(PBu^n_3)_8$ and $OPBu^n_3$; this signified that oxidative elimination of two tri(n-butyl)phosphine ligands had occurred to give $Pd_{23}(CO)_{20}(PBu^n_3)_8$ and the phosphine oxide byproduct. In order to ascertain the resulting hypothesis of chemically induced *reversible* interconversions in solution between these two structurally unalike Pd_{23} clusters, the corresponding triethylphosphine **1** and **2** were chosen, based upon the facts that pure **1** and **2** are easier to prepare and that crystal structure determinations had been performed for both **1** and **2**.

Herein are presented results of a $^{31}P\{^1H\}$ NMR investigation revealing that $Pd_{23}(CO)_{20}(PEt_3)_{10}$ (**1**) and $Pd_{23}(CO)_{20}(PEt_3)_8$ (**2**), which stoichiometrically differ by only two phosphines, can indeed be chemically induced in solution to interconvert reversibly into one another. A four-stage structural diagram which preserves maximum connectivities is presented that shows a *hypothetical intramolecular* transformation of **1** into **2** upon removal of the two phosphine ligands. Although *intermolecular* cluster-disassembly/cluster-assembly processes are well-known for generating higher nuclearity palladium carbonyl phosphine clusters and cannot be ruled out, nevertheless this *least-nuclear-motion* [18] scheme reveals the geometrical relationship between the two dissimilar Pd_{23} cores of **1** and **2**.

These chemically-induced reversible interconversions between $Pd_{23}(CO)_{20}(PEt_3)_{10}$ (**1**) and $Pd_{23}(CO)_{20}(PEt_3)_8$ (**2**) also belong to the third class and provide the first example among palladium carbonyl phosphine clusters where phosphine removal (or addition) from certain metal site(s) in the cluster causes a large metal-core rearrangement with *retention* of the metal-core nuclearity.

Results and discussion

Geometrical features of Pd_{23} cores in $Pd_{23}(CO)_{20}(PEt_3)_{10}$ (1) and $Pd_{23}(CO)_{20}(PEt_3)_8$ (2)

(a) $Pd_{23}(CO)_{20}(PEt_3)_{10}$ (1). Its metal-core geometry in Fig. 1(a) consists of a centered Pd_{13} cuboctahedron of 13 Pd(*n*) atoms [*n* = 1 (interior), 4–15] along with six additional (square-face)-capping Pd(*n*) atoms (*n* = 2, 3, 16–19) and four edge-capping wingtip Pd(*n*) atoms (*n* = 20–23).[6,7,11,15] The centered hexacapped Pd_{19} cuboctahedron may alternatively be viewed as a centered ν_2 Pd_{19} octahedron (where ν_n designates (*n* + 1) equally spaced atoms along each edge) of O_h symmetry.[11,15] The four wingtip Pd(*n*) atoms (*n* = 20–23) lie on one of the octahedral mirror planes such that the molecular symmetry is reduced to D_{2h}. Addition of the 10 PEt_3 ligands that are attached to the six tetracapping and four wingtip Pd atoms along with 16 doubly bridging μ_2-COs and four triply bridging μ_3-COs preserves the idealized D_{2h} geometry. Because both the tetracapping and wingtip Pd atoms are each composed of $Pd(CO)_2(PEt_3)$ units, the resulting composition of **1** may be formulated as $Pd_{13}\{Pd(CO)_2(PEt_3)\}_{10}$ as well as $Pd_{23}(CO)_{20}(PEt_3)_{10}$.

Table 1 Mean Pd–Pd connectivities under pseudo-D_{2d} symmetry in known $Pd_{23}(CO)_{20}(PEt_3)_8$ [a] (**2**) and triisopropylphosphine analogue (**2a**) [b,c] and corresponding individual ranges for **2**

Connectivity [def]	*N* [g]	Mean [e]/Å	Range/Å
Pd(1)–Pd(2)	2	2.82 (2.73)	2.81–2.83
Pd(1)–Pd(4)	8	2.92 (2.90)	2.90–2.94
Pd(1)–Pd(8)	4	2.97 (2.99)	2.94–3.01
Pd(5)–Pd(6)	4	2.81 (2.79)	2.74–2.84
Pd(4) ··· Pd(5)	4	4.06 (4.16)	4.03–4.11
Pd(4) ··· Pd(12)	4	3.22 (3.10)	3.19–3.26
Pd(2)–Pd(4)	8	2.78 (2.80)	2.74–2.82
Pd(8)–Pd(4)	8	2.70 (2.68)	2.68–2.71
Pd(8)–Pd(12)	8	2.73 (2.73)	2.70–2.75
Pd(2)–Pd(20) [h]	4	2.80 (2.78)	2.78–2.82
Pd(8)–Pd(20) [h]	4	2.68 (2.67)	2.67–2.68
Pd(5)–Pd(20) [h]	4	2.84 (3.15)	2.80–2.88
Pd(4)–Pd(16)	8	2.72 (2.73)	2.68–2.76

[a] Atomic coordinates were obtained from Professor Yuri Slovokhotov (Nesmeyanov Institute of Organoelement Compounds, Russian Academy of Science, Moscow, Russia); private communication to L. F. Dahl, June, 2002. [b] Ref. 10*b*. [c] Means for the $P(Pr^i_3)$ analogue are given in parentheses. [d] Atom-labeling is given in Fig. 1. [e] Under assumed D_{2d} symmetry there are six different types of Pd(*n*) atoms; the following Pd(*n*) atoms in Fig. 1 are symmetry-equivalent: *n* = 1; *n* = 2, 3; *n* = 4–7, 12–15; *n* = 8–11; *n* = 16–19; *n* = 20–23. [f] Bonding connectivities are denoted by solid lines; nonbonding connectivities by three horizontal dots. [g] *N* denotes the number of symmetry-equivalent connectivities under D_{2d} symmetry. [h] The highly asymmetrically tetracapped Pd(*n*) atoms (*n* = 20–23) conform closely to S_4 instead of D_{2d} symmetry.

(b) $Pd_{23}(CO)_{20}(PEt_3)_8$ (2). The closely similar Pd_{23} core-geometries of **2** in Figs. 1(b) and (c) and its triisopropylphosphine analogue (**2a**) may be viewed as a highly deformed centered hexacapped cubic Pd_{15} kernel of 15 Pd(*n*) atoms [*n* = 1 (interior), 4–7, 12–15, 2, 3, 8–11] that is linked to four two-connected (wingtip) $Pd(\mu_2\text{-}CO)_2(PR_3)$ fragments (*n* = 16–19) and likewise to four three-connected $Pd(\mu_2\text{-}CO)_2(PR_3)$ fragments (*n* = 20–23). Each of the remaining four carbonyl ligands is a triply bridging μ_3-CO that is asymmetrically coordinated to an open triangular face of the Pd_{15} kernel: namely, to two of the eight cubic corner Pd(*n*) atoms (*n* = 4–7, 12–15) and one of the four side tetracapping Pd(*n*) atoms (*n* = 8–11). The Pd_{15} kernel ideally has tetragonal D_{2d} symmetry (Table 1). Individual values of Pd–Pd distances for **2** expectedly show closer adherence to D_{2d} symmetry than those for **2a**; the generally smaller dispersions of individual Pd–Pd distances for each of the means in **2** together with the observed variations between corresponding means in **2** and **2a** being large for only two types of Pd–Pd bonding connectivities (Table 1) can be readily attributed to steric effects being considerably greater in **2a** due to the larger tri(isopropyl)phosphine ligands.

The central Pd(1) atom of the Pd_{15} kernel is coordinated by two shorter and 12 somewhat longer bonding connectivities to the other 14 kernel atoms: namely, connected to the two *trans* Pd(*n*) atoms (*n* = 2, 3) (mean, 2.82 Å) and connected to the eight vertex Pd(*n*) atoms (*n* = 4–7; 12–15) of the highly deformed cube (mean, 2.92 Å) and to the other four *cis* Pd(*n*) atoms (*n* = 8–11) that each cap the greatly distorted cubic Pd_4 side faces (mean, 2.97 Å). The exceedingly large molecular deformation of this centered hexacapped cubic Pd_{15} kernel from a regular cubic O_h geometry to the observed pseudo-D_{2d} geometry may be formally achieved by the top and bottom "square" faces being extensively elongated in perpendicular directions. These two polygonal Pd_4 faces [*n*(top) = 4–7; *n*(bottom) =

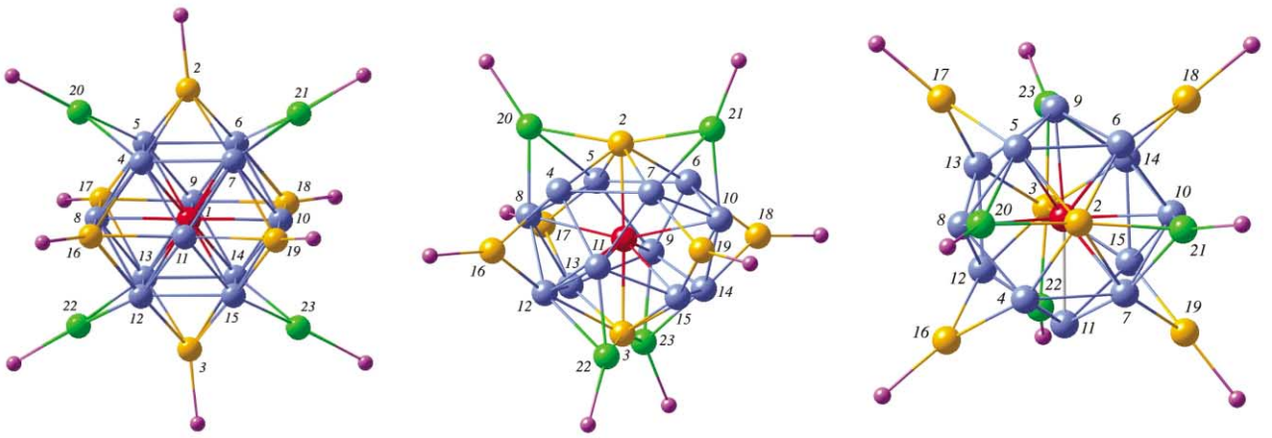

(a) $Pd_{23}(CO)_{20}(P)_{10}$ (b) $Pd_{23}(CO)_{20}(P)_8$, side (c) $Pd_{23}(CO)_{20}(P)_8$, top

Fig. 1 Palladium-phosphorus frameworks of (a) $Pd_{23}(CO)_{20}(PEt_3)_{10}$ (**1**) and of (b), (c) $Pd_{23}(CO)_{20}(PEt_3)_8$ (**2**) that stoichiometrically differ only by two additional PEt_3 ligands attached to Pd(2) and Pd(3) in **1**. Atom-numbering establishes the structural relationship of the D_{2h} Pd_{23} core in **1** with the D_{2d} Pd_{23} core in **2**. Atom-coloring is based upon the centered hexacapped cuboctahedral geometry of $Pd_{23}(CO)_{20}(PEt_3)_{10}$ (**1**). View (a) shows that the $Pd_{23}(P)_{10}$ fragment in **1** possesses a centered Pd_{13} cuboctahedral kernel consisting of an interior Pd(1) atom (red) coordinated to 12 ccp Pd(*n*) atoms (blue). This Pd_{13} kernel of O_h symmetry is capped on each of its six square faces by Pd(*n*) atoms (*n* = 2, 3, 16–19; gold); the four remaining exopolyhedral edge-capping (wingtip) Pd(*n*) atoms (*n* = 20–23; green) located on a cuboctahedral mirror plane lower the symmetry from O_h to D_{2h}. Ten phosphorus atoms (violet) are attached to the six tetracapping and four wingtip Pd atoms. The nearly perpendicular views (b) and (c) show that the $Pd_{23}(P)_8$ fragment in **2** may be described as a highly distorted centered hexacapped cubic Pd_{15} arrangement of 14 atoms (2 gold; 12 blue) connected to the centered Pd(1) atom (red); for clarity, connectivities are drawn between the interior Pd(1) atom (red) and two tetracapping axial Pd(2), Pd(3) atoms (gold) and four tetracapping horizontal Pd(*n*) atoms (*n* = 8–11; blue) but *not* between Pd(1) and eight geometrically deformed cubic corner Pd(*n*) atoms (*n* = 4–7, 12–15; blue). In turn, this Pd_{15} kernel is linked to four two-connected (wingtip) capping Pd(*n*) atoms (*n* = 16–19; gold) and four three-connected capping Pd(*n*) atoms (*n* = 20–23; green). The overall $Pd_{23}(P)_8$ geometry ideally conforms to tetragonal D_{2d} symmetry with the improper S_4 axis passing through the centered Pd(1) (red) and Pd(2), Pd(3) (gold). View (c) approximately down the S_4 axis reveals that one of the two perpendicular σ_d mirror planes (that bisect the perpendicular pair of horizontal twofold axes) passes through Pd(*n*) with *n* = 1, 2, 3, 9, 11, 22, 23 and the other σ_d through Pd(*n*) with *n* = 1, 2, 3, 8, 10, 20 and 21. This idealized metal-core conformity of **2** to D_{2d} symmetry is based upon the inherent assumption that the four Pd(*n*) atoms (*n* = 20–23) related by the S_4 axis can be viewed as tetracapping instead of tricapping connected atoms (see text).

12–15] each evolve into two *trans bonding* and two *trans non-bonding* cubic edges that are related to each other by an improper S_4 rotatory-reflection axis (which includes a proper C_2 axis) that passes through the centered Pd(1) atom and the two axially (*trans*) tetracapped Pd(2) and Pd(3) atoms; each of the initially four "square" *non-bonding* Pd_4 side faces concomitantly is transformed into one bonding and three non-bonding cubic edges. The eight remaining palladium atoms form particular capping connectivities with the Pd_{15} kernel; these are composed of: (1) four two-connected wingtip Pd(*n*) atoms (*n* = 16–19) that span the four non-bonding vertical cubic Pd–Pd edges and thereby preserve the pseudo-D_{2d} symmetry; and (2) four Pd(*n*) atoms (*n* = 20–23) that may be considered as tetracapping atoms; each is positioned above a completely bonding square-like Pd_4 face of the Pd_{15} kernel composed of one of the two axially tetracapping Pd(*n*) atoms (*n* = 1, 2), one of the four resulting horizontal tetracapping Pd(*n*) atoms (*n* = 8–11), and two of the eight Pd(*n*) atoms (*n* = 4–7, 12–15) comprising the highly deformed cube. However, this tetracapping of each Pd(*n*) atom (*n* = 20–23) is highly asymmetric; one of the four Pd–Pd distances is much longer (>3.2 Å) than the other three bonding distances (with means of 2.68, 2.80, and 2.84 Å) and is thereby considered to be non-bonding. This highly asymmetric tetracapping lowers the symmetry of the entire Pd_{23} core-geometry of **2** from D_{2d} to S_4. Similar asymmetric open μ_3-Pd face-capping of Pd(μ_2-CO)$_2$(PEt_3) fragments (with one much longer Pd–Pd distance) has been observed in capped octahedral palladium clusters.[15]

Possible intramolecular structural interconversion between $Pd_{23}(CO)_{20}(PEt_3)_{10}$ (1) and $Pd_{23}(CO)_{20}(PEt_3)_8$ (2)

A hypothetical stage-by-stage intramolecular rearrangement of the Pd_{23} core in **1** into Pd_{23} core in **2** that retains maximum connectivities is presented in Fig. 2. The driving force for this rearrangement is the removal of two phosphine ligands from the two *trans* (axial) Pd(2), Pd(3) atoms lying on the two-fold axis of the D_{2h} centered hexacapped Pd_{19} cuboctahedron (**1**) shown in Fig. 1a. Because of the resulting coordination unsaturation, the axial Pd(2) and Pd(3) atoms are each markedly shifted from non-bonding distances toward the centered Pd(1); the ensuing formation of Pd(2)–Pd(1) and Pd(3)–Pd(1) bonding interactions (mean, 2.82 Å) necessitates a dramatic expansion of the top and bottom initially edge-bonding "square" Pd_4 faces of the Pd_{13} cuboctahedron (blue) in perpendicular directions; in turn, this gives rise to cleavage of two of the four edge-bonding Pd–Pd connectivities in each of the top and bottom formerly cubic square Pd_4 faces in **1** (*viz*., rupturing of Pd(4) ··· Pd(5), Pd(6) ··· Pd(7), Pd(12) ··· Pd(15), and Pd(13) ··· Pd(14) connectivities in Fig. 1a).

Major consequences are:

(1) each of the four gold Pd(*n*) kernel atoms (*n* = 16–19) of the Pd(CO)$_2$(PEt_3) units that tetracap the four equatorial "square" Pd_4 side faces of the Pd_{13} cuboctahedron in **1** undergoes bond-cleavage with the two horizontal cubic blue Pd(*n*) atoms (*n* = 8,11; 8,9; 9,10; 10,11) and thereby becomes a two-connected wingtip atom in **2**; these four wingtip atoms essentially remain in the horizontal plane with the central Pd(1) but are displaced further away from the central Pd(1) such that their resulting *non-bonding* Pd(1) ··· Pd(*n*) distances (*n* = 16–19) are increased from a mean of 3.93 Å in **1** to 4.70 Å in **2**. Each of the other four equatorial cuboctahedral blue kernel Pd(*n*) atoms (*n* = 8–11) in **1** likewise undergoes bond-scission with its two neighboring equatorial Pd(*n*) atoms (*n* = 16–19) that tetracap two adjacent side cubic square faces in **1**; in turn, these four Pd(*n*) atoms in **2** each form a bonding connectivity with one of the formerly green wingtip Pd atoms (*n* = 20–23) in **1** but maintain linkage to the resulting four highly distorted cubic Pd_4 side faces in **2**.

(2) The relative angular orientation of the two pairs of wingtip (edge-bridging) Pd(μ_2-CO)$_2$(PEt_3) units in **1** [*viz*., Pd(20), Pd(21) and Pd(22), Pd(23)] changes from being

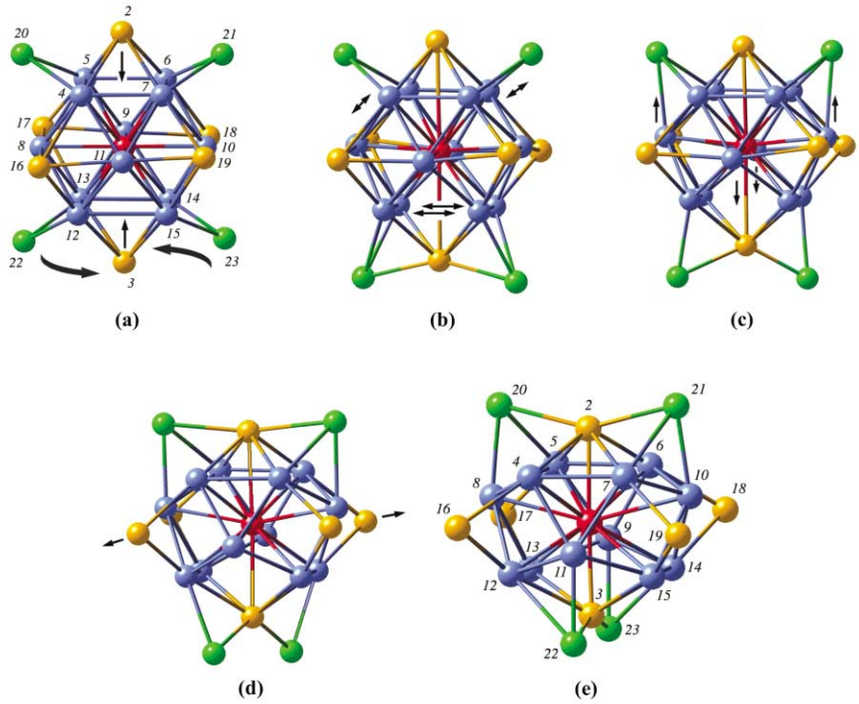

Fig. 2 Four-stage structural diagram showing the geometrical relationship between the structurally dissimilar Pd_{23} cores of $Pd_{23}(CO)_{20}(PEt_3)_{10}$ (**1**) and $Pd_{23}(CO)_{20}(PEt_3)_8$ (**2**). Although possible *inter*molecular, transformations have not been experimentally excluded, this hypothetical, geometrical transformation illustrates the possible *intra*molecular pathway that preserves maximum connectivities upon removal of the two phosphine ligands *via* reaction with O_2 (air). Stages (**a**) and (**e**) correspond to the metal-core geometries of **1** and **2**, respectively, with the same numbering of corresponding atoms as presented in Fig. 1 for both structures. Arrows point to the types of structural distortions. Bond-cleavage of two PEt_3 ligands from *trans*, tetracapping Pd(2), Pd(3) atoms (gold) of the D_{2h} Pd_{23} core-geometry in **1** and resulting formation of the D_{2d} Pd_{23} core-geometry in **2** are proposed to proceed from stage (**a**) to stage (**e**) by intermediate snapshot stages (**b**)–(**d**). Although the stages in this least-nuclear-motion scheme are shown consecutively, the occurrence of an *intra*molecular transformation would no doubt involve an essentially simultaneous combination (*i.e.*, concerted process) of all stages. Each stage-transformation involves the formation and scission of particular atom-pair connectivities. (1) (**a**) to (**b**) transformation: 1–2; 1–3; 3–22; 3–23 connectivities formed. 4 ··· 5; 6 ··· 7; 13 ··· 14; 12 ··· 15 connectivities broken. (2) (**b**) to (**c**) transformation: 8–20; 10–21 connectivities formed. 22 ··· 13; 23 ··· 15 connectivities broken upon commencement of counterclockwise 90° rotation of connected Pd(22)–Pd(3)–Pd(23) fragment about the S_4 Pd(3)–Pd(1)–Pd(2) axis. (3) (**c**) to (**d**) transformation: continuation of 90° rotation of connected Pd(22)–Pd(3)–Pd(23) fragment about the S_4 axis. 2–20; 2–21 connectivities formed. 4 ··· 20; 6 ··· 21; 8 ··· 16,17; 9 ··· 17,18; 10 ··· 18,19; 11 ··· 16,19 connectivities broken. (4) (**d**) to (**e**) transformation: completion of 90° rotation of Pd(22)–Pd(3)–Pd(23) fragment about S_4 axis. 22–11; 23–9 connectivities formed. The total number of Pd–Pd bonding connectivities has significantly decreased in the formation of **2**, from 68 in **1** to 62 in **2**. Noteworthy is that mean Pd–Pd bonding connectivities range from 2.68 to 2.97 Å; mean Pd–Pd distances >3.22 Å are designated as non-bonding connectivities. This arbitrary distinction gives rise to the formulation of four wingtip (edge-capping) $Pd(\mu_2\text{-}CO)_2(PR_3)$ fragments in both **1** and **2** and four tricapping $Pd(\mu_2\text{-}CO)_2(PR_3)$ fragments (n = 20–23) in **2**.

"planar" in **1** to being perpendicularly disposed with respect to each other in **2**; this resulting perpendicular disposition of the two pairs in **2** is accomplished in Fig. 2 by a counterclockwise 90° rotation of the bottom connected Pd(22)–Pd(3)–Pd(23) fragment about the S_4 Pd(2)–Pd(1)–Pd(3) axis in **2** (*i.e.*, C_2 in **1**). These two pairs of edge-capping $Pd(CO)_2(PEt_3)$ units [*i.e.*, Pd(20), Pd(21) and Pd(22), Pd(23)] in **1** also change their coordination neighbors; instead of edge-capping opposite sides of the top and the bottom "square" faces in **1**, each of these Pd atoms in **2** now has three-connected bonding interactions. Irrespective of the actual mechanistic pathway, this geometrical correlation provides a logical interconnection between their otherwise seemingly unrelated metal-core geometries.

$^{31}P\{^1H\}$ NMR study of chemically induced interconversions between $Pd_{23}(CO)_{20}(PEt_3)_{10}$ (1) and $Pd_{23}(CO)_{20}(PEt_3)_8$ (2)

(a) General comments. Based upon prior demonstrations by Mednikov[1,16,17] that phosphine ligands in palladium carbonyl phosphine clusters can be readily oxidized to phosphine oxide, O_2 (air) was chosen as the phosphine-removal reagent to convert **1** into **2**. "Free" phosphine was then used to convert **2** back into **1**.

$$Pd_{23}(CO)_{20}(PEt_3)_{10}\ (\mathbf{1}) + O_2 \longrightarrow Pd_{23}(CO)_{20}(PEt_3)_8\ (\mathbf{2}) + 2\ Et_3PO$$

$$Pd_{23}(CO)_{20}(PEt_3)_8\ (\mathbf{2}) + 2PEt_3 \longrightarrow Pd_{23}(CO)_{20}(PEt_3)_{10}\ (\mathbf{1})$$

$^{31}P\{^1H\}$ NMR measurements used to monitor these transformations indicated the formation of a third known cluster, $Pd_{16}(CO)_{13}(PEt_3)_9$ (**3**),[4] in the conversion of **2** into **1**, if an excess of PEt_3 was used. The palladium-phosphorus framework of **3** of crystallographic C_3 symmetry is displayed in Fig. 3.[4] Its geometry can be described as a centered $Pd_{13}(\mu_3\text{-}CO)_7(PEt_3)_6$ icosahedron with three additional exopolyhedral wingtip $Pd(\mu_2\text{-}CO)_2(PEt_3)$ fragments that edge-bridge three equatorial Pd–Pd bonds of the icosahedron.[19]

(b) Spectral characterization. All $^{31}P\{^1H\}$ spectra with applied 2 Hz line-broadening were recorded on a Bruker-300 MHz spectrometer, in C_6D_6 solvent; 85% H_3PO_4 in D_2O was used as an external standard. All three clusters, $Pd_{23}(CO)_{20}(PEt_3)_{10}$ (**1**), $Pd_{23}(CO)_{20}(PEt_3)_8$ (**2**), and $Pd_{16}(CO)_{13}(PEt_3)_9$ (**3**), were synthesized in accordance with published procedures.[4,6b,10a] Solutions for NMR experiments were prepared by use of 7–10 mg (1.5–2.5 μmol) of each cluster. The ambient temperature $^{31}P\{^1H\}$ NMR spectrum of **1** (C_6D_6) consists of three resonances at δ 6.2 (br s, 2P), 4.8 (t, 4P), and 3.3 (s, 4P) ppm with ^3J(P–P) = 3.6 Hz. The ambient temperature $^{31}P\{^1H\}$ NMR spectrum of **2** (C_6D_6) has two equivalent singlet resonances at δ 13.9 and 9.6 ppm; no coupling between resonances or even line-broadening was detected in the spectrum. The ambient temperature $^{31}P\{^1H\}$ NMR spectrum of **3** (C_6D_6) consists of two doublets and one singlet of equal intensities; the doublets are centered at δ 18.2 (3P) and

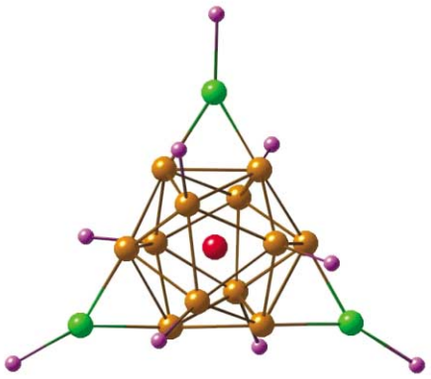

Fig. 3 Palladium-phosphorus framework of the known $Pd_{16}(CO)_{13}(PEt_3)_9$ cluster[4] showing the central atom (red) encapsulated by an icosahedral Pd_{12} cage (brown) with three additional exopolyhedral edge-bridged (wingtip) Pd atoms (green). Alkyl substituents on phosphorus atoms (violet) and eight doubly and five triply bridging carbonyl ligands are omitted.

−0.8 (3P) ppm [^3J(P–P) = 30 Hz], and the singlet is positioned at δ −1.1 (3P) ppm.

(c) Chemically induced conversion of $Pd_{23}(CO)_{20}(PEt_3)_8$ (2) into $Pd_{23}(CO)_{20}(PEt_3)_{10}$ (1). Reactions of **2** in C_6D_6 solution with different quantities of added PEt_3 in an NMR tube were monitored by use of $^{31}P\{^1H\}$ NMR spectra. The initial spectrum corresponded to **2** together with some Et_3PO; this impurity is not active in this studied process and consequently does not affect the results. Upon addition of 0.3 μL of PEt_3 (2.2 μmol) to **2**, an NMR spectrum after 10 min revealed the appearance of the three resonances corresponding to **1** along with a very small signal at δ −1.1 ppm, which was assigned to **3**. Addition of the second portion of 0.3 μL of PEt_3 to **2** followed by a waiting period of 10 min again yielded a decrease in the signals of **2**. After 5 h of storage under Ar, a third portion of excess PEt_3 (1.2 μL) was added; a spectrum recorded after 10 min showed complete conversion of **2** into **1**. Throughout the period when spectra were recorded, no large change in the signal of **3** was observed. However, once the complete conversion of **2** into **1** was achieved, partial conversion of product **1** into **3** and other unidentified products occurred over a time-span of 10 h at room temperature.

The results from this study clearly demonstrate fast and complete conversion of **2** into **1** upon treatment with added "free" PEt_3 together with a much slower and incomplete conversion of product **1** into **3**, if an excess of PEt_3 is added. These observed reactions can be summarized in the two following equations:

$$Pd_{23}(CO)_{20}(PEt_3)_8\,(\mathbf{2}) + 2PEt_3 \xrightarrow{\text{fast}} Pd_{23}(CO)_{20}(PEt_3)_{10}\,(\mathbf{1})$$

$$Pd_{23}(CO)_{20}(PEt_3)_{10}\,(\mathbf{1}) + PEt_3 \xrightarrow{\text{slow}} Pd_{16}(CO)_{13}(PEt_3)_9\,(\mathbf{3})$$

In order to evaluate competition between the rate of reaction of O_2 (air) with **1** *versus* that of PEt_3 with **2**, a $^{31}P\{^1H\}$ NMR spectrum of **1**, prepared in air, was recorded, and then 0.4 μL of PEt_3 (~2-fold excess) were added directly into the NMR tube. Subsequent $^{31}P\{^1H\}$ NMR spectra of the reaction (upon PEt_3 addition) were obtained after 10 min, 24 h, and 48 h. The solution was then sealed (with air) and stored in the refrigerator. The interpreted data revealed that an excess of PEt_3 quickly converts **2** into **1** even in air. However, prolonged exposure of product **1** to O_2 (air) completely reconverts **1** into **2**. No formation of **3** was indicated from spectral data in this experiment, indicating that conversion of product **1** into **3** under an excess of PEt_3 is a much slower process than the complete transformation of **2** into **1**.

Attempts to convert $Pd_{23}(CO)_{20}(PEt_3)_8$ (**2**) into mixed phosphine-ligated analogues of **1**, $Pd_{23}(CO)_{20}(PEt_3)_8(PR_3)_2$ (where R = PBu_3^n or PPh_3) were not successful. Addition of 0.2 μL of PBu_3^n or 0.2 mg of PPh_3 (in THF-d_6 solution) to **2** resulted in the appearance of weak resonances very close to the signals of **1**. This is indicative of PR_3 (R = PBu_3^n, PPh_3) having been substituted for PEt_3 ligands in **2**, but *not* the addition of PR_3 to **2** to obtain the mixed phosphine-ligated **1**. The observance of very weak resonances corresponding only to the triethylphosphine-ligated **1** appeared after the addition of PR_3 (R = Bu^n, Ph) to the solution. These observations imply a secondary reaction involving the formation of **1** from "free" PEt_3 that was replaced by PR_3 in **2**, as given by the equations:

$$\underset{\mathbf{2}}{Pd_{23}(CO)_{20}(PEt_3)_8} + xPR_3 \rightarrow \underset{\text{mixed phosphine ligated } \mathbf{2}}{Pd_{23}(CO)_{20}(PEt_3)_{8-x}(PR_3)_x} + xPEt_3$$

$$\tfrac{x}{2}\,\underset{\mathbf{2}}{Pd_{23}(CO)_{20}(PEt_3)_8} + xPEt_3 \rightarrow \tfrac{x}{2}\,\underset{\mathbf{1}}{Pd_{23}(CO)_{20}(PEt_3)_{10}}$$

The non-addition of PR_3 (R = PBu_3^n, PPh_3) to **2** to form the mixed phosphine-ligated **1** can be presumably rationalized in terms of initial steric repulsion arguments; this would suggest that "free" PBu_3^n or PPh_3 ligands would encounter significantly greater steric repulsion from neighboring PEt_3 ligands relative to that of "free" PEt_3 ligands upon approaching the reaction centers [assumed to be P(2), P(3) in **2** for the proposed intramolecular interconversion]. Nevertheless, it is noteworthy that the well-known Tolman cone angle is the same for a "bound" PEt_3 or PBu_3^n ligand (132°) and larger for a "bound" PPh_3 ligand (143°).[20a] However, under these circumstances a major problem arises in the use of assigned steric parameter values for different "bound" PR_3 ligands that are obtained either from geometric constructs such as the widely used Tolman cone-angle model or from calculated ligand repulsive energy parameters (E_rs) based upon a molecular mechanics model (from which the E_r values for "bound" PEt_3, PBu_3^n, and PPh_3 ligands are 61, 64, and 75 kcal mol^{-1}, respectively).[20b] It was pointed out[20b] that these steric parameters, which generally assume that the "ligand-bound" conformation gives the smallest cone angle may not be good approximations for certain "free" PR_3 ligands (as in the cases of PEt_3 and PBu_3^n). Furthermore, the existence and stability of the PBu_3^n analogue of **1**, which can readily be synthesized from other reactions,[6a,c] implies that the experimentally indicated non-conversion of **2** into the mixed PEt_3/PBu_3^n-ligand analogue of **1** is most likely due to kinetics rather than thermodynamics. In contrast to PBu_3^n, the PPh_3 analogue of **1** has not been synthesized to date; its non-existence (as yet) may likewise be a consequence of kinetics rather than thermodynamics.

(d) Chemically induced conversion of $Pd_{23}(CO)_{20}(PEt_3)_{10}$ (1) into $Pd_{23}(CO)_{20}(PEt_3)_8$ (2). Room-temperature reactions of a C_6D_6 solution of **1** in an NMR tube with O_2 (air) were performed under different conditions and again monitored by use of $^{31}P\{^1H\}$ NMR spectra. After a solution of **1** was exposed to air for 10 s, a $^{31}P\{^1H\}$ NMR spectrum exhibited a decrease in the signals of **1** along with the appearance of small resonances corresponding to the signals of **2**. Signals of **3** were present in the initial spectrum of **1** as an impurity. The description below of the behavior of the mixture of **1** and **3** under air was also checked independently by separate use of purified **1** and **3**; the observed results were identical. After the solution of **1** was exposed to air for 60 s, its signals decreased even further, while those of **3** were essentially unaffected. An additional purging of the solution with 10 mL of air displayed pronounced decreases in the signals of **1** and increases in those of **2** and Et_3PO after 30 min. Complete conversion of **1** into **2** occurred after a

10 hour-storage in a refrigerator upon additional exposure to air; the signal of **3** also decreased. Subsequent storage for 24 h at room temperature resulted in the complete conversion of **1** and **3** into **2** and Et_3PO.

The results from this study also demonstrate a fast, complete conversion of **1** into **2** upon exposure to the atmospheric oxygen. If an excess of air was used, a much slower but complete conversion of **3** into **2** was also observed. These results are summarized in the following equations:

$$Pd_{23}(CO)_{20}(PEt_3)_{10}(\mathbf{1}) + O_2 \xrightarrow{\text{fast}} Pd_{23}(CO)_{20}(PEt_3)_8(\mathbf{2}) + 2Et_3PO$$

$$Pd_{16}(CO)_{13}(PEt_3)_9(\mathbf{3}) + O_2 \xrightarrow{\text{slow}} Pd_{23}(CO)_{20}(PEt_3)_8(\mathbf{2}) + Et_3PO$$

Scheme of interconversions among 1, 2, and 3

Fig. 4 presents a diagram that summarizes the interconversion(s) among **1**, **2**, and **3**. Addition of "free" PEt_3 to **2** quickly converts it into **1**. If an excess of PEt_3 is added, product **1** slowly transforms into **3**. Addition of O_2 (air) to **1** quickly converts it into **2**, but the rate of reaction is not nearly as fast as the conversion of **2** into **1**; an excess of O_2 (air) slowly converts **3**, if present in the reaction mixture, into **2**. The relatively slow rates of reactions involving **3** are presumably caused by complex structural rearrangements in that the icosahedral-based Pd_{16} nuclearity in **3** is different from the identical Pd_{23} nuclearities in **1** and **2**. Consequently, both the reaction of **1** with excess PEt_3 to form **3** and the reaction of **3** with O_2 (air) to form **2** are not quantitative, in contrast to the chemically-induced interconversion reactions between **1** and **2**. As the cycle is repeated, unidentified products accumulate in the reaction medium. This diagram shows that it is still unclear whether **2** can be directly transformed into **3** without first going through the formation of product **1**, in that **1** forms much faster than **3**.

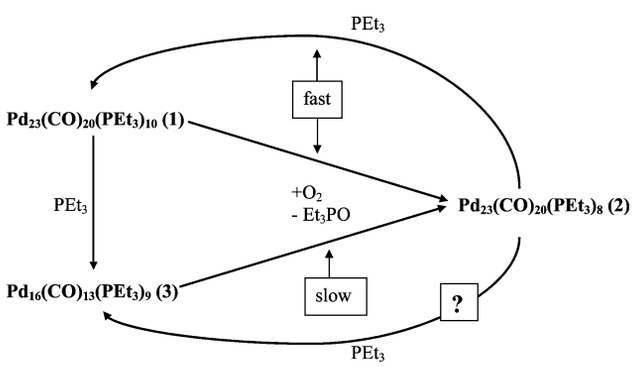

Fig. 4 Diagram summarizing observed interconversions among **1**, **2**, and **3**.

These facile interconversions strikingly illustrate the marked increased capability of CO/PR_3-ligated palladium clusters (relative to those of other Group 8–10 elements) to undergo large changes in metal-core geometries upon addition/removal of ligands. This exceptional behavior may be readily ascribed to the markedly different nature of Pd–Pd and Pd–CO bonding interactions.

Acknowledgements

This research was supported by the National Science Foundation (CHE-9729555). Departmental purchase of the Varian UNITY-500 NMR was partially made possible by funds from NSF CHE-9629688 and of the Bruker AC-300 NMR by funds from NSF CHE-9208963 and NIH 1 SIO RRO8389–01. We gratefully acknowledge Dr Charles Fry (UW-Madison) for experimental NMR assistance. We also are greatly indebted to Professor Yuri Slovokhotov (Nesmeyanov Institute of Organoelement Compounds, Russian Academy of Sciences, Moscow, Russia) who furnished the atomic coordinates and lattice parameters of the well-refined crystal structure of $Pd_{23}(CO)_{20}(PEt_3)_8$ (**2**). Color figures were prepared with Crystal Maker, Interactive Crystallography (version 5). David C. Palmer (P.O. Box 183 Bicester, Oxfordshire, UK OX6 7BS).

References and notes

1 (*a*) $Pd_{10}(CO)_{12}(PR_3)_6$ (R = Bu^n, Et): E. G. Mednikov and N. K. Eremenko, *Izv. Akad. Nauk SSSR, Ser. Khim.*, 1982, 2540 (*Russ. Chem. Bull.*, 1982, **31**, 2240) (*Engl. Trans.*); (*b*) $Pd_{10}(CO)_{14}(PBu^n_3)_4$: E. G. Mednikov, N. K. Eremenko, Yu. L. Slovokhotov, Yu. T. Struchkov and S. P. Gubin, *J. Organomet. Chem.*, 1983, **258**, 247; (*c*) $Pd_{10}(CO)_{12}(PPh_3)_6$: E. G. Mednikov and N. K. Eremenko, *Izv. Akad. Nauk SSSR, Ser. Khim.*, 1984, 2781 (*Russ. Chem. Bull.*, 1984, **33**, 2547) (*Engl. Trans.*); (*d*) $Pd_{10}(CO)_{12}(PEt_3)_6$: D. M. P. Mingos and C. M. Hill, *Croat. Chim. Acta*, 1995, **68**(4), 745; (*e*) E. G. Mednikov, Ph.D. Thesis, Moscow State University, 1983.

2 $Pd_{12}(CO)_{12}(PBu^n_3)_6$: E. G. Mednikov, Yu. T. Struchkov and Yu. L. Slovokhotov, *J. Organomet. Chem.*, 1998, **566**, 15.

3 $Pd_{12}(CO)_{12}(PPh_3)_6$, $[Pd_{29}(CO)_{28}(PPh_3)_7]^{2-}$: M. Kawano, J. W. Bacon, C. F. Campana, B. E. Winger, J. D. Dudeck, S. A. Sirchio, S. L. Scruggs, U. Geiser and L. F. Dahl, *Inorg. Chem.*, 2001, **40**, 2554.

4 $Pd_{16}(CO)_{13}(PEt_3)_9$: E. G. Mednikov, Yu. L. Slovokhotov and Yu. T. Struchkov, *Metalloorg. Khim.*, 1991, **4**, 123 (*Organomet. Chem. USSR*, 1991, **4**, 65) (*Engl. Trans.*).

5 $Pd_{16}(CO)_{13}(PMe_3)_9$, $Pd_{35}(CO)_{23}(PMe_3)_{15}$, $Pd_{39}(CO)_{23}(PMe_3)_{16}$, $Pd_{59}(CO)_{32}(PMe_3)_{21}$: N. T. Tran, M. Kawano and L. F. Dahl, *J. Chem. Soc., Dalton Trans.*, 2001, 2731.

6 $Pd_{23}(CO)_{22}(PEt_3)_{10}$: (*a*) E. G. Mednikov, N. K. Eremenko, Yu. L. Slovokhotov and Yu. T. Struchkov, *J. Organomet. Chem.*, 1986, **301**, C35; E. G. Mednikov, *Metalloorg. Khim.*, 1991, **4**, 885 (*Organomet. Chem. USSR*, 1991, **4**, 433) (*Engl. Trans.*); (*b*) $Pd_{23}(CO)_{20}(PEt_3)_{10}$: J. Wittayakun, N. T. Tran, D. R. Powell and L. F. Dahl, manuscript in preparation; (*c*) $Pd_{23}(CO)_{20}(PBu^n_3)_{10}$: E. G. Mednikov, S. A. Ivanov and L. F. Dahl, unpublished research, 2000; (*d*) $Pd_{23}(CO)_{21}(PEt_3)_{10}$: E. G. Mednikov, L. F. Dahl, unpublished research, 2002.

7 Reactions by Wittayakun *et al.*[6b] of the $[Pd_{13}Ni_{13}(CO)_{34}]^{4-}$ tetraanion[8] with PEt_3 in the presence of acid produced, in addition to the known Pd_{10}, Pd_{16}, and Pd_{34} clusters,[1a,d,4,9] $Pd_{23}(CO)_{20}(PEt_3)_{10}$[6b] that has the same Pd_{23} framework as that previously reported by Mednikov *et al.*[6a] for $Pd_{23}(CO)_{22}(PEt_3)_{10}$ but with two fewer COs. Repeated attempts recently made by Mednikov[6d] to obtain the original crystal form [*viz.*, monoclinic, $P2_1/n$; Z = 2 with each molecule possessing C_i ($\bar{1}$) site symmetry] containing the 22 CO-ligated cluster have instead only afforded the different crystal form [*viz.*, tetragonal, $I4_1/a$; Z = 8 with each molecule having C_2 (2) site symmetry] of the 20 CO-ligated cluster; a comparative qualitative molecular analysis[6b] favors the existence of both clusters. A recent X-ray crystallographic analysis[6c] showed that the originally formulated cuboctahedral-based tributylphosphine $Pd_{23}(CO)_{22}(PBu^n_3)_{10}$[6a] is instead $Pd_{23}(CO)_{20}(PBu^n_3)_{10}$ with 20 bridging carbonyl ligands. Furthermore, from other reactions Mednikov[6d] recently obtained another crystal form of the cuboctahedral-based triethylphosphine Pd_{23} cluster with 10 PEt_3 ligands but with 21 carbonyl ligands.

8 N. T. Tran, M. Kawano, D. R. Powell and L. F. Dahl, *J. Chem. Soc., Dalton Trans.*, 2000, 4138.

9 (*a*) $Pd_{34}(CO)_{24}(PEt_3)_{12}$, $Pd_{38}(CO)_{28}(PR_3)_{12}$ (R = Et, Bu^n): E. G. Mednikov and N. I. Kanteeva, *Izv. Akad. Nauk SSSR, Ser. Khim.*, 1995, 167 (*Russ. Chem. Bull.*, 1995, **44**, 163) (*Engl. Trans.*); (*b*) $Pd_{38}(CO)_{28}(PEt_3)_{12}$: E. G. Mednikov, N. K. Eremenko, Yu. L. Slovokhotov and Yu. T. Struchkov, *J. Chem. Soc., Chem. Commun.*, 1987, 218.

10 (*a*) $Pd_{23}(CO)_{20}(PEt_3)_8$: E. G. Mednikov, N. K. Eremenko, Yu. L. Slovokhotov and Yu. T. Struchkov, *Zh. Vses. Khim. Ova. im. D. I. Mendeleeva*, 1987, **32**, 101 (in Russian): E. G. Mednikov, *Izv. Akad. Nauk SSSR, Ser. Khim.*, 1993, 1299 (*Russ. Chem. Bull.*, 1993, **42**, 1242) (*Engl. Trans.*); (*b*) $Pd_{23}(CO)_{20}(PPr^i_3)_8$: J. Wittayakun, Ph.D. Thesis, 2000, UW-Madison, WI.

11 $Pd_{30}(CO)_{26}(PEt_3)_{10}$, $Pd_{54}(CO)_{40}(PEt_3)_{14}$: E. G. Mednikov, S. A. Ivanov and L. F. Dahl, *Angew. Chem., Int. Ed.*, 2003, **42**, 323.

12 $Pd_{52}(CO)_{36}(PEt_3)_{14}$, $Pd_{66}(CO)_{48}(PEt_3)_{16}$: E. G. Mednikov, S. A. Ivanov, I. A. Guzei and L. F. Dahl, *Abstracts of Papers, 222nd ACS National Meeting of the American Chemical Society*, Chicago, IL, American Chemical Society, Washington, DC, Aug. 2001, INORG 331.

13 $Pd_{59}(CO)_{32}(PMe_3)_{21}$: N. T. Tran, M. Kawano, D. R. Powell and L. F. Dahl, *J. Am. Chem. Soc.*, 1998, **120**, 10986.
14 $Pd_{145}(CO)_x(PEt_3)_{60}$: N. T. Tran, D. R. Powell and L. F. Dahl, *Angew. Chem., Int. Ed.*, 2000, **39**, 4121.
15 (*a*) N. K. Eremenko, E. G. Mednikov and S. S. Kurasov, *Russ. Chem. Rev.*, 1985, **54**, 394; and references therein; (*b*) N. K. Eremenko and S. P. Gubin, *Pure Appl. Chem.*, 1990, **62**, 1179; (*c*) R. B. King, *Gazz. Chim. Ital.*, 1992, **122**, 383; (*d*) A. D. Burrows and D. M. P. Mingos, *Transition Met. Chem.*, 1993, **18**, 129 and references therein.
16 E. G. Mednikov, N. K. Eremenko, S. P. Gubin, Yu. L. Slovokhotov and Yu. T. Struchkov, *J. Organomet. Chem.*, 1982, **239**, 401.
17 This $^{31}P\{^1H\}$ NMR spectrum in C_6D_6 at room temperature (external std.: 85% H_3PO_4 in D_2O) displayed signals at δ 4.3 (s), 0.2 (s), −4.7 (s), and 40.2 (s) ppm with intensity ratios 3.8 : 4.0 : 1.5 : 2.4, respectively; these signals were unambiguously ascribed to pure $Pd_{23}(CO)_{20}(PBu^n_3)_8$ [δ 4.3 (s, 4P), 0.2 (s, 4P) ppm (no coupling observed)] and Bu^n_3PO [δ 40.2 (s) ppm]; the signal at −4.7 ppm was not identified.
18 S. Ehrenson, *J. Am. Chem. Soc.*, 1974, **96**, 3778; S. Ehrenson, *J. Am. Chem. Soc.*, 1974, **96**, 3784 and references therein.
19 The crystallographically analyzed trimethylphosphine analogue, $Pd_{16}(CO)_{13}(PMe_3)_9$, is isostructural with **3** (ref. 5).
20 (*a*) C. A. Tolman, *Chem. Rev.*, 1977, **77**, 313; (*b*) T. L. Brown and K. J. Lee, *Coord. Chem. Rev.*, 1993, **128**, 89; T. L. Brown, *Inorg. Chem.*, 1992, **31**, 1286 and references therein.